Crystal Structures of *Escherichia coli* RecA in Complex with MgADP and MnAMP−PNP[†,‡]

Xu Xing and Charles E. Bell*

Department of Molecular and Cellular Biochemistry, Ohio State University College of Medicine and Public Health, 371 Hamilton Hall, 1645 Neil Avenue, Columbus, Ohio 43210

Received August 25, 2004; Revised Manuscript Received October 4, 2004

ABSTRACT: RecA catalyzes the DNA pairing and strand-exchange steps of homologous recombination, an important mechanism for repair of double-stranded DNA breaks. The binding of RecA to DNA is modulated by adenosine nucleotides. ATP increases the affinity of RecA for DNA, while ADP decreases the affinity. Previously, the crystal structures of *E. coli* RecA and its complex with ADP have been determined to resolutions of 2.3 and 3.0 Å, respectively, but the model for the RecA−ADP complex did not include magnesium ion or side chains. Here, we have determined the crystal structures of RecA in complex with MgADP and MnAMP−PNP, a nonhydrolyzable analogue of ATP, at resolutions of 1.9 and 2.1 Å, respectively. Both crystals grow in the same conditions and have RecA in a right-handed helical form with a pitch of ∼82 Å. The crystal structures show the detailed interactions of RecA with the nucleotide cofactors, including the metal ion and the γ phosphate of AMP−PNP. There are very few conformational differences between the structures of RecA bound to ADP and AMP−PNP, which differ from uncomplexed RecA only in a slight opening of the P-loop residues 66−73 upon nucleotide binding. To interpret the functional significance of the structure of the MnAMP−PNP complex, a coprotease assay was used to compare the ability of different nucleotides to promote the active, extended conformation of RecA. Whereas ATPγS and ADP−AlF_4 facilitate a robust coprotease activity, ADP and AMP−PNP do not activate RecA at all. We conclude that the crystal structure of the RecA−MnAMP−PNP complex represents a preisomerization state of the RecA protein that exists after ATP has bound but before the conformational transition to the active state.

RecA is a DNA-dependent ATPase that is the central player in bacterial homologous recombination, an essential mechanism in all cells for repair of double-stranded DNA (dsDNA) breaks (*1*, *2*). When presented with single-stranded DNA (ssDNA), RecA−adenosine 5′-triphosphate (ATP)[1] polymerizes on the DNA, forming a right-handed helical filament called the presynaptic complex. In a poorly understood reaction that occurs within the RecA nucleoprotein filament, the ssDNA is paired with a complementary strand of duplex DNA and a strand-exchange reaction proceeds with unidirectional branch migration. The RecA−ATP−ssDNA presynaptic complex is also a cofactor for the self-cleavage of LexA and related phage repressors, events that initiate the SOS response and induction of lytic phage growth, respectively (*3*, *4*). This function of RecA is called coprotease activity. The structural features of RecA−DNA complexes have been extensively characterized by electron microscopy (EM; *5*), and the X-ray crystal structures of *Escherichia coli* RecA (*6*) and its complex with ADP (*7*) have been determined in the absence of DNA but in a helical form that closely resembles that seen for RecA−DNA complexes by EM.

The binding of RecA to DNA is controlled by adenosine nucleotides; ATP increases the affinity of RecA for ssDNA, whereas ADP decreases its affinity (*8*). DNA stimulates the ATPase activity of RecA to a maximal rate of ∼30 min^{-1}. Nonhydrolyzable ATP analogues such as ATPγS and ADP−AlF_4 also enhance the DNA-binding of RecA, but optimal strand-exchange activity requires ATP hydrolysis. EM studies of RecA−DNA filaments reveal essentially two conformational states of the protein. A compressed, "inactive" filament with a helical pitch of ∼70 Å is seen in the presence of ADP or no nucleotide, while a more extended, "active" conformation, with a pitch of ∼95 Å is seen in the presence of ATP or ATP analogues (*5*). Crystal structures of bacterial RecA, which have helical pitches of 67−83 Å, are generally thought to represent the compressed, inactive state of the protein (*6*−*7*, *9*−*13*). However, the structure of the individual protomers and the interactions between them that are seen in the crystals are likely to be important conformations that occur during the catalytic cycle of the strand-exchange reaction. Recent improved EM reconstructions of RecA−DNA complexes reveal that in the extended, active conformation each protomer is reoriented from its position in the crystal

[†] This work was supported by NIH GM 067947 and ACS IRG-98-278-02 to C.E.B.

[‡] The coordinates of the RecA−MgADP and RecA−MnAMP−PNP structures have been deposited in the Protein Data Bank under accession numbers 1XMV and IXMS, respectively.

* To whom correspondence should be addressed. E-mail: bell.489@osu.edu. Telephone: (614) 688-3115. Fax: (614) 292-4118.

[1] Abbreviations: ATP, adenosine 5′-triphosphate; ADP, adenylyl 5′-diphosphate; ATPγS, adenosine 5′-*O*-(3-thiotriphosphate); AMP−PNP, 5′-adenylyl imidodiphosphate; EM, electron microscopy; Mt, *Mycobacterium tuberculosis*; Ms, *Mycobacterium smegmatis*; Dr, *Deinococcus radiodurans*; λcI_{93-236}, residues 93−236 of the λ repressor.

10.1021/bi048165y CCC: $27.50
Published on Web 12/04/2004

structure, such that the ATP site moves to the subunit interface (*14*). Although this conformational change has not yet been observed in crystal structures of RecA, very recent crystal structures of yeast Rad51 (*15*) and archaeal RadA (*16*), which are RecA counterparts, reveal extended filaments with the ATP site at the subunit interface, just as is seen for RecA at lower resolution by EM. Although the details remain poorly understood, the emerging picture is that ATP binding, hydrolysis, and release control subunit movements and other conformational changes within the RecA filament that are somehow coupled to the protein−DNA interactions that promote the DNA strand-exchange reaction (*17*).

The 2.3 Å crystal structure of uncomplexed RecA provided a framework for interpreting a wealth of genetic and biochemical data (*6*). Briefly, RecA folds into an N-terminal domain (residues 1−33) that packs against the neighboring subunit in the filament, a core domain (residues 34−269) that has the ATP and primary ssDNA- and dsDNA-binding sites, and a C-terminal domain (residues 270−352) that has a site for binding dsDNA (*18*). The regions of RecA thought to be principally involved in DNA binding are two loops L1 (residues 157−164) and L2 (residues 195−209) of the core domain (*19*), which are not resolved in the crystal structure but point toward the central axis of the filament, where the DNA is known to bind (*20*). The overall fold of the RecA core domain is seen in a diverse group of proteins that couple the energy of ATP binding and hydrolysis to promoting mechanical processes. This structural family, for which RecA is the founding member, includes DNA helicases (*21*), F1 ATP synthase (*22*), ABC transporters (*23*−*24*), and the Rad50 DNA repair enzyme (*25*). Thus, a common structural scaffold has evolved to couple ATP-mediated conformational changes to a diverse array of cellular processes.

The ATP-binding site on RecA was identified by soaking ADP into crystals of RecA alone, and the structure of the RecA−ADP complex was determined to 3.0 Å (*7*). However, the model for RecA−ADP did not include magnesium ion or side chains, and thus, the detailed interactions between the protein and nucleotide have not been characterized. Crystal structures of RecA from *Mycobacterium tuberculosis* (MtRecA) and *M. smegmatis* (MsRecA) have been determined at resolutions of 3.0−3.8 Å in the presence of various adenosine nucleotides, including ADP−AlF_4, ATPγS, and dATP (*9*−*11*). These structures are in a helical form with a pitch of ∼74 Å and are otherwise very similar to the *E. coli* RecA structures. Notably, even though there is no DNA in the crystals, the DNA-binding loops L1 and L2 are each resolved in at least one of the structures of MtRecA, although not together in a single structure. Although the ordering of the loops is apparently affected by the presence of magnesium and the adenosine nucleotides, the precise mechanism for this is not clear. The structure of RecA from *Deinococcus radiodurans* (DrRecA) has been determined at 2.5 Å resolution in complex with ATPγS in a helical filament with a pitch of 67 Å (*13*). None of the bacterial RecA structures includes the magnesium ion that coordinates the phosphates and is essential for activity. All of these structures have RecA in a compressed helical filament with the ATP-binding site facing the central axis of the filament, away from the subunit interface, as seen in the original *E. coli* RecA structure.

E. coli RecA has been a model system, not only for DNA strand-exchange enzymes but also for a broad family of enzymes that coordinate ATP binding and hydrolysis with promoting mechanical events. Despite this central importance, the high-resolution structures of the relevant adenosine nucleotide complexes of *E. coli* RecA have not been determined. Here, we present the crystal structures of *E. coli* RecA in complex with MgADP and MnAMP−PNP, a nonhydrolyzable analogue of ATP, at resolutions of 1.9 and 2.1 Å, respectively. Although also in the compressed, inactive conformation, the structures show the detailed interactions between the protein and nucleotides and for the first time for RecA include the bound metal ion. We also present data from a coprotease assay comparing the ability of various ATP analogues to promote the activated conformation of the RecA−DNA filament, which helps in interpreting the functional significance of the structures. Together, the structural and biochemical data suggest that the MnAMP−PNP complex seen in the crystal structure represents a preisomerization state of the protein.

EXPERIMENTAL PROCEDURES

Protein Expression, Purification, and Crystallization. RecA was expressed from a pET14b vector (Novagen) and purified as has been described (*12*). The purified protein has the extra sequence Gly-Ser-His-Met at the N terminus. Residues 93−236 of the λ repressor (λcI_{93-236}) were expressed and purified as has been described for $\lambda cI_{132-236}$ (*26*). All crystals were grown at 22 °C by hanging drop vapor diffusion. For the RecA−MgADP complex, the reservoir solution consisted of 45% ethylene glycol and 100 mM MES at pH 6.0 and the hanging drop was prepared by mixing 2 μL of reservoir solution with 2 μL of 10 mg/mL RecA, 20 mM Tris-HCl at pH 8.0, 1 mM dithiothreitol, 10 mM NaF, 4 mM $MgCl_2$, and 2 mM ADP. For the RecA−MnAMP−PNP complex, the reservoir solution consisted of 36% ethylene glycol and 0.1 M MES at pH 6.0 and the hanging drop was prepared by mixing 2 μL of reservoir solution with 2 μL of 10 mg/mL RecA, 20 mM Tris-HCl at pH 8.0, 2 mM AMP−PNP, and 4 mM $MnCl_2$.

X-ray Data Collection, Structure Determination, and Refinement. Crystals were mounted in nylon loops (Hampton Research) directly from the hanging drops and frozen in liquid nitrogen. X-ray diffraction data for the RecA−MgADP complex were collected at beamline 19-ID at the Advanced Photon Source using a CCD detector and processed using HKL2000 (*27*). X-ray diffraction data for the RecA−MnAMP−PNP complex were collected using a Rigaku RUH3RHB rotating anode generator and an RAXIS-IV++ image plate detector and processed using CrystalClear software (Molecular Structure Corporation). Structures were determined by molecular replacement using the original RecA crystal structure (PDB code 2REB; *6*) as a search model. Molecular replacement was performed with the AMoRe program (*28*) of the CCP4 package (*29*). Crystallographic refinement used the CNS software (*30*), with the overall anisotropic temperature factor, bulk solvent corrections to the data, and a maximum-likelihood target. Refinement included rigid-body minimization, simulated annealing, conjugate-gradient minimization, and individual *B*-factor protocols. A total of 10% of the data was used for the calculation of the free *R* factor. Model building used the

program O (*31*). Figures were prepared using MOLSCRIPT (*32*), RASTER3D (*33*), and O.

Coprotease Assays. The coprotease assay used SDS−PAGE to monitor the self-cleavage of a fragment of the λ repressor (λcI_{93-236}) in the presence of RecA, ssDNA, and adenosine nucleotides. All reactions were performed at 22 °C. Each reaction (50 μL) contained 10 μM RecA, 30 μM (nucleotides) 15-mer ssDNA oligonucleotide with the sequence 5′-TGGTGGTGGTGGTGG-3′ (University of Pennsylvania Nucleic Acid Facility), 5 μM λcI_{93-236}, 20 mM Tris-HCl at pH 7.4, 2 mM $MgCl_2$, and 50 mM NaCl. The 15-mer ssDNA was added to a 1:1 binding site ratio with RecA (1 RecA molecule binds 3 nucleotides of DNA). As indicated, some reactions contained 1 mM ADP or 1 mM ATPγS. Reactions with ADP−AlF_4 contained 1 mM ADP, 2 mM $Al(NO_3)_3$, and 10 mM NaF. Reactions with ADP−BeFx contained 1 mM ADP, 2 mM $BeCl_2$, and 10 mM NaF. Reactions with ADP−vanadate contained 1 mM ADP and 3 mM sodium vanadate. Reactions with pyrophosphate contained 3 mM sodium pyrophosphate. For each reaction, all of the components except λcI_{93-236} were mixed and incubated for 30 min before the reactions were initiated by the addition of λcI_{93-236}. Aliquots of the reactions were removed at each of the indicated time points, and the reactions were stopped by adding 0.25 volume of 5× SDS−PAGE loading buffer and heated to 95 °C for 5 min. Samples were run on 13.5% SDS−PAGE gels and stained with Coomassie brilliant blue.

RESULTS AND DISCUSSION

Crystal Growth and Properties. The RecA protein used in this study was purified as an N-terminal 6His-fusion protein. After removal of the 6His tag by thrombin cleavage, the purified RecA protein contains the extra residues Gly-Ser-His-Met at the N terminus. This protein, hereafter referred to as RecA, has ssDNA-dependent coprotease and ATPase activities that are indistinguishable from native RecA (data not shown). RecA−MgADP and RecA−MnAMP−PNP were crystallized at pH 6.0 from ∼40% ethylene glycol solutions with 100 mM MES buffer and no salt. The X-ray crystal structures of the complexes were determined by molecular replacement to 1.9 and 2.1 Å, respectively (Table 1), using the original RecA structure (PDB code 2REB; *6*) as a starting structure. In the crystals, RecA forms a perfectly 6_1-symmetric helical filament with a pitch of ∼82 Å (Figure 1). There is one monomer of RecA in the asymmetric unit of the crystal. This crystal form, which we will call form 5, is very similar to that reported for the original RecA crystal structure, called form 1, but with some key differences. Aside from being produced from significantly different solution conditions, form 1 crystals were grown in the absence of nucleotide (*6*, *34*). In contrast, form 5 crystals do not grow at all in the absence of adenosine nucleotide. Whereas the form 5 crystals grow within 2 days in the presence of MgADP or MgAMP−PNP, they do not grow initially in the presence of ATPγS or ADP−AlF_4 but appear after ∼3 weeks, presumably because of slow hydrolysis of ATPγS or oxidation of aluminum. The electron density in the active-site region, determined from crystals grown with ATPγS and $ADPAlF_4$ appears identical to the MgADP complex, and these crystals were not pursued further. Manganese could be substituted for magnesium, and in the case of the RecA−AMP−PNP complex, the electron density in the active-site region was more optimal with the manganese ion. Thus, the MnAMP−PNP structure is reported here. The crystals do not grow in the presence of dADP, ADP−VO_4, ADP−BeF_x, or pyrophosphate. The adenosine nucleotide-binding site is distant from the crystal-lattice contacts; therefore, the effects of the different compounds on crystal growth apparently arise from their influence on the overall conformation of the RecA filament.

Table 1: Crystal Data and Refinement Statistics

crystal data	RecA−Mg−ADP	RecA−Mn−AMP−PNP
space group	$P6_1$	$P6_1$
$a = b$ (Å)[a]	100.5	100.7
c (Å)	82.2	81.9
resolution (Å)	50.0−1.9	38.5−2.1
number observed	372 954	123 176
number unique	37 004	26 179
completeness (%)	99.1 (100.0)[b]	94.8 (66.3)
redundancy	10.1 (9.8)	4.7 (2.1)
R_{merge} (%)[c]	5.3 (53.3)	5.0 (32.9)
I/σ	62.4 (6.5)	18.4 (2.9)
refinement statistics		
resolution (Å)	50−1.9	38.5−2.1
number reflections (working/free)	32 073/3555	23 586/2587
completeness (%)	95.7	94.8
rmsd from ideality		
bonds (Å)	0.005	0.005
angles (deg)	1.1	1.2
R factor/free R factor (%)[d]	20.2/23.5	22.4/26.2
modeled residues	3−156	3−156
	172−194	167−195
	213−328	212−328
number of water molecules	197	124

[a] For comparison, the unit cell dimensions of the form 1 crystal are $a = b = 102.4$ Å and $c = 82.7$ Å and the resolution is 2.3 Å. [b] Numbers in parentheses refer to the highest resolution shell only. [c] $R_{merge} = \sum|I_h - \langle I\rangle_h|/\sum I_h$, where $\langle I\rangle_h$ is the average intensity over symmetry equivalents. [d] R factor $= \sum|F_{obs} - F_{calc}|/\sum F_{obs}$. The free R factor is calculated from 10% of the reflections that are omitted from the refinement.

On the basis of the crystallization properties, we conclude that the crystal form 5 presented here represents specifically the ADP-bound state of the protein, which is also consistent with the AMP−PNP-bound state. Although AMP−PNP binds to RecA, it apparently does not elicit the conformational transition to the activated filament strongly enough to disrupt the crystal-lattice contacts. In contrast, ATPγS and ADP−AlF_4 induce the conformational transition to the extended, activated filament, which is incompatible with the form 5 crystal-lattice contacts. Consistent with this interpretation, soaking of ATP or ATPγS into crystals of the RecA−MgADP complex results in their immediate shattering, as has been observed previously with the form 1 crystals (*34*).

Effect of Different Adenosine Nucleotides on RecA Coprotease Activity. To further interpret the effects of the various adenosine nucleotides on the crystallization of RecA, we used a coprotease assay to test the ability of the different nucleotides to induce the activated conformation of RecA. Binding of LexA and related phage repressors to RecA−ssDNA−ATP filaments results in the self-cleavage of the repressors at a specific peptide bond, between Ala111 and Gly112 in the case of the λ repressor. The extended RecA−ssDNA−ATP complex forms a docking site for repressor molecules that stabilizes them in a cleavage-competent

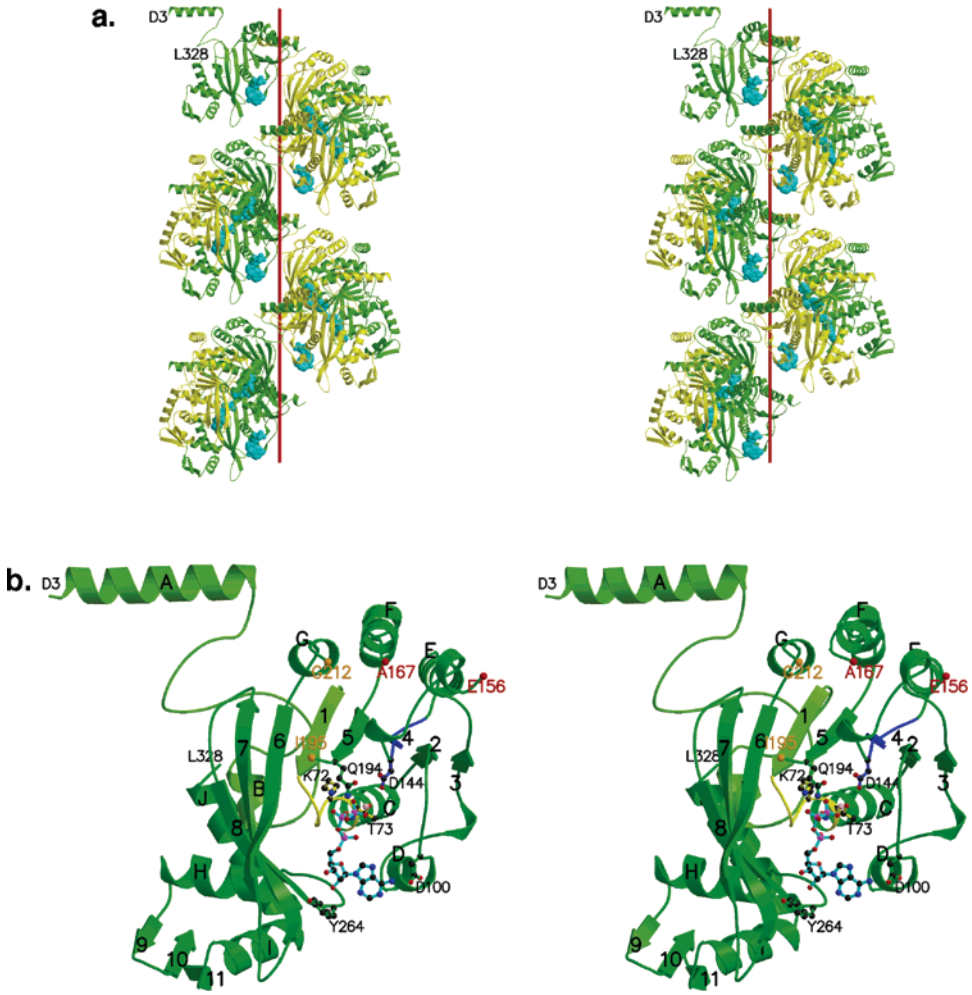

FIGURE 1: Structure of the RecA−MnAMP−PNP complex. (a) Stereoview of two complete turns of the RecA helical filament, with alternating subunits colored green and yellow and AMP−PNP in cyan. The view is perpendicular to the filament axis (crystallographic *c* axis), which is shown as a red line. The 5′ end of ssDNA would be bound at the top of the filament in this orientation. The N- and C-terminal residues of the model are labeled for the uppermost monomer of the filament. Notice that the bound AMP−PNP faces the central axis of the filament and does not contact the neighboring subunit. (b) Stereoview of a monomer of the RecA−MnAMP−PNP complex. The orientation is approximately the same as for the uppermost monomer of the filament in a. AMP−PNP and the side chains of key residues of RecA that contact AMP−PNP are shown in a ball-and-stick model. The Walker A motif, residues 66−73, is colored yellow, and the Walker B motif, residues 139−144, is colored blue. The flanking residues of the two disordered loops L1 and L2 are indicated by the red and orange spheres and labels. The manganese ion is a pink sphere near T73. α helices and β strands are labeled according to Story et al. (*6*).

conformation. Thus, the formation of the extended RecA−ssDNA−ATP filament can be assessed indirectly by monitoring the cleavage of a repressor protein. Here, SDS−PAGE is used to monitor the self-cleavage of residues 93−236 of the λ repressor (λcI_{93-236}) in the presence of RecA, a 15-mer ssDNA, and different adenosine nucleotides (Figure 2). ATPγS and ADP−AlF_4 strongly activate the coprotease activity of RecA, resulting in ∼50% cleavage of λcI_{93-236} within about 15 min and 100% cleavage within 24 h. Interestingly, there is consistently more cleavage in the presence of ADP−AlF_4 than with ATPγS, implying that the transition-state analogue is somewhat better at promoting the active conformation of the RecA−ssDNA complex. ADP and AMP−PNP are not able to activate the coprotease activity of RecA at all; even after 24 h, there is no detectable cleavage of λcI_{93-236}. Similarly, pyrophosphate, ADP−VO_4, ADP−BeF_x, and the absence of adenosine nucleotide all result in no detectable cleavage after 24 h (data not shown). We conclude that like ADP, AMP−PNP does not promote the extended, active conformation of RecA that is observed in the presence of ATP, ATPγS, or ADP−AlF_4. It has been reported that AMP−PNP increases the affinity of RecA for ssDNA, although not to the same extent as ATPγS (*8*). AMP−PNP has been shown to produce an extended conformation of RecA−DNA filaments, as seen by EM (*14*). It may be that AMP−PNP does not elicit the extended conformation of RecA strongly enough to overcome the crystal-packing forces or promote coprotease activity. It is also conceivable that AMP−PNP causes specific structural alterations in the RecA−ssDNA complex that somehow disrupt coprotease activity toward λcI_{93-236}.

Overall Structures. The structures of the RecA−MgADP and RecA−MnAMP−PNP complexes reported here (Figure 1) are overall very similar to one another and to the structure of uncomplexed *E. coli* RecA. Monomers from the RecA−MgADP and RecA−MnAMP−PNP structures can be superimposed to an root-mean-square deviation (rmsd) of 0.16 Å for all main-chain atoms or 0.15 Å for the core domains only. Superimposing the structure of uncomplexed *E. coli* RecA (PDB code 2REB) to the MgADP complex gives an

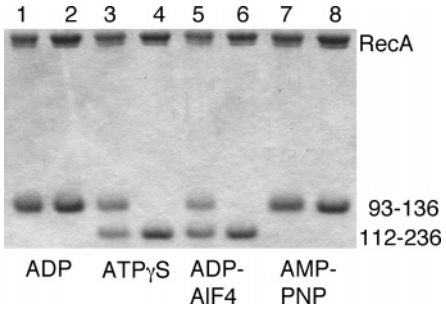

FIGURE 2: Ability of different adenosine nucleotides to promote RecA coprotease activity. The coprotease activity of RecA (M_r = 38 255) is measured by the cleavage of λcI_{93-236} (M_r = 16 388) to $\lambda cI_{112-236}$ (M_r = 13 725). Self-cleavage of λcI_{93-236} occurs specifically at the Ala111-Gly112 peptide bond and is dependent on its association with the extended, active form of the RecA−ssDNA filament. Results of reactions with ADP (lanes 1 and 2), ATPγS (lanes 3 and 4), ADP−AlF_4 (lanes 5 and 6), and AMP−PNP (lanes 7 and 8) are shown. Lanes 1, 3, 5, and 7 are samples from each reaction after 15 min, and lanes 2, 4, 6, and 8 are after 24 h. Notice that while ATPγS and ADP−AlF_4 lead to ~50% cleavage of λcI_{93-236} within 15 min, ADP and AMP−PNP result in no cleavage even after 24 h. Also notice by comparing lanes 3 and 5 that the rate of cleavage with ADP−AlF_4 is slightly faster than with ATPγS.

rmsd of 0.39 Å for all main-chain atoms (0.34 Å for the core domains only) or to the MnAMP−PNP complex gives an rmsd of 0.37 Å for all main-chain atoms (0.28 Å for the core domains only). The only significant conformational change in the protein caused by adenosine nucleotide binding is a slight opening of the P loop (residues 66−73) such that the main-chain atoms of Glu68 and Thr73 each move by ~1 Å, in opposite directions, away from one another. The widening of the P loop is seen for both the MgADP and MnAMP−PNP complexes and for other RecA structures in which the active site is occupied by a nucleotide or by a sulfate or phosphate ion (*9*−*13*). Although the functional significance of this conformational change is not known, it could conceivably be important for relaying information on the occupancy of the active site to the DNA-binding regions of the molecule. In addition, because the P loop is near the monomer−monomer interface in the active form of the RadA−MnANP−PNP filament (*16*), the nucleotide-dependent opening of the P loop could have some role in controlling the monomer−monomer interactions throughout the strand-exchange reaction.

Essentially the same amino acid residues of RecA that are disordered in the original structure are also disordered in the structures of the complexes reported here. These are the N-terminal residues 1−2 (plus the extra GSHM residues that are from the vector), residues of the two principal DNA-binding loops L1 and L2 (residues 157−164 and 195−209), and the C-terminal "tail" residues 329−352 (Table 1). There are no differences in the orientation of the C-terminal domain, which was seen to vary slightly in crystal forms of *E. coli* RecA in a more compressed helical filament (*12*). The ATP-binding site is not at the subunit interface, as is seen by EM for the extended conformation of RecA−DNA complexes (*14*), but rather points toward the central axis of the filament, as in previous RecA structures (*6*−*7*, *8*−*13*). Finally, there is no significant change in the monomer−monomer interactions or in the interfilament-bundling interactions. Thus, aside from the presence of the adenosine nucleotides and the slight opening of the P loop, the structures of the complexes reported here are essentially the same as the original structure of uncomplexed RecA (*6*).

Structure of the RecA−MgADP Complex. The electron density corresponding to the bound ADP is complete, allowing for accurate placement of the entire cofactor (Figure 3). There is also a strong peak for the associated magnesium ion, confirmed by an MnADP − MgADP (F_{obs} − F_{obs}) difference Fourier electron density map, which shows an 18 σ peak near the position of the magnesium ion. As seen previously at a lower resolution (*7*), there are five regions of the RecA polypeptide that protrude into the active site to interact with the bound MgADP. First, the P loop, also called the Walker A motif, forms intimate interactions with the magnesium ion and the phosphates. The sequence of the P loop in *E. coli* RecA (residues 66−73) is GPESSGKT and is identical in 57 of 63 eubacterial RecA sequences (*35*). The magnesium ion is coordinated with near octahedral geometry by the Oγ1 hydroxyl of Thr73, the β phosphate of ADP, and 4 water molecules. The side chain of Thr73 does not fit the observed electron density well (Figure 3a), indicating some distortion or disorder that is difficult to model accurately from the 1.9 Å resolution data, possibly because of its close proximity to the magnesium ion. The negatively charged phosphates of ADP are neutralized by the magnesium ion, Lys72 of the P loop, and a helix dipole interaction with the N-terminal end of helix C, which immediately follows the P loop. The phosphates of ADP form hydrogen bonds to six consecutive backbone amide groups (residues 69−74) of the P loop, as well as to the side chains of Ser70, Lys72, Thr73, and Thr74. The intimate interaction of the phosphates with the backbone atoms of the P loop agrees well with the observation that a version of RecA protein bearing a P loop with the sequence GAAAAGKT (four consecutive alanine substitutions) retains 90% of the recombinase activity of native RecA protein (*36*). The side chains of Glu68 and Ser69 of the P loop, which are invariant across 63 eubacterial RecA sequences (*35*) and sensitive to amino acid substitutions (*37*), do not contact ADP (or AMP−PNP) but instead point out into the solvent. Their functional importance is not apparent from the present structures; although they point toward the central axis of the filament, it has been suggested that they may contact the DNA.

A second region of RecA important for adenosine nucleotide binding is the Walker B motif, residues 139−144. Although this region is highly conserved among a wide variety of ATP-binding proteins, it does not make direct contact with ADP or AMP−PNP. Asp144 of the Walker B motif approaches to within 4.0 Å of the magnesium and binds directly to Thr73 (one of the magnesium ligands) and one of the water molecules coordinated to the magnesium. As seen for the corresponding sequence in all RecA and related structures, the Asp144-Ser145 peptide bond of the Walker B motif is clearly in the rare cis conformation. A third region of RecA that contacts the ADP is residues 96−103, which form a loop and the beginning of helix D. Residues of this segment, in particular His97, also participate in interactions at the subunit interface in the filament. Glu96, which is thought to be the catalytic base in the ATPase reaction, interacts with a water molecule that is near the magnesium ion and also contacts Ser145 of the Walker B motif. Residues 97−99 extend along one side of the ADP-binding pocket without making any direct contacts with ADP. There is strong

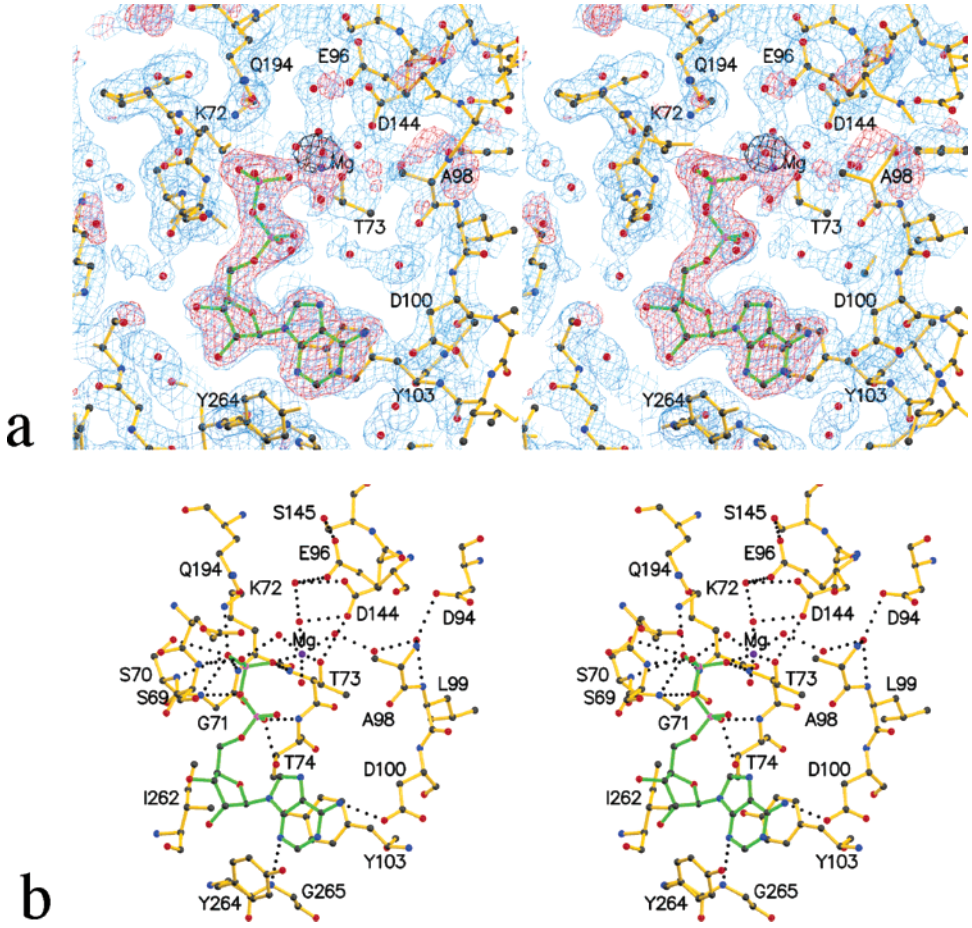

FIGURE 3: Interactions between RecA and MgADP. (a) Stereoview of electron density in the vicinity of the bound MgADP. The blue cage is a 1.9 Å $2F_{obs} - F_{calc}$ electron density map, contoured at 1 σ. The red cage is a simulated annealing $F_{obs} - F_{calc}$ omit map, contoured at 3 σ, in which the magnesium and ADP were omitted. The black cage is a RecA−MnADP − RecA−MgADP difference Fourier map ($F_{obs} - F_{obs}$) contoured at 10 σ, showing a peak overlapping the position of the magnesium ion. The view is roughly the same as in Figure 1b. (b) Stereoview of atomic interactions between RecA and MgADP. Potential hydrogen bonds within 3.5 Å are shown as dotted lines. Notice the octahedral coordination of the magnesium and that the phosphates of ADP form hydrogen bonds with six consecutive amide groups of the P loop.

electron density for 3 water molecules that bridge the magnesium ion with the backbone amide groups of Ala98 and Leu99 and the carboxylate of Asp94 (Figure 3a). Interestingly, the electron density shows some evidence of an alternate conformation for the backbone of Ala98, which lies about 7 Å from the magnesium ion. Although it was not possible to accurately model this alternative conformation, it appears to involve a hydrogen bond between the backbone carbonyl oxygen of Ala98 and the side chain of Asp94, a residue that is invariant but does not participate directly in interactions with ADP. Conceivably this flexibility could be indicative of a conformational change that is more prevalent in other states of the enzyme. Moving further along this segment, Asp100 forms a close hydrogen bond with the N6 amino group of the adenine ring of ADP, which is stacked on top of Tyr103. Asp100 plays a key role in dictating the specificity of RecA for adenosine nucleotides (*38*). It is near this region of the structure that the ADP makes its closest approach to the neighboring subunit, in the 5′ direction of the filament. Residues Gln257, Lys245, and Arg243, which are on the $\beta7-\beta8$ hairpin of the neighboring subunit, are about 6 Å from the adenine ring in this conformation of the filament. In the crystal structure of an extended form of a RadA−MgAMP−PNP complex, similarly positioned residues of the neighboring subunit form an "ATP-cap" motif that closes over the adenine and ribose rings of AMP−PMP (*16*).

A fourth region of RecA that contacts the ATP is residues 262−265, which form a tight turn between the last β strand ($\beta8$) of the core domain and the first helix (helix H) of the C-terminal domain (Figure 1b). Conceivably, this segment could be important in relaying conformational changes from the ATP site to the C-terminal domain, which have been observed by EM (*39*). Ile262 packs against the back of the ribose ring; Tyr264 packs against the adenine ring; and the backbone amide of Gly265 is within hydrogen-bonding distance of the N3 atom of the adenine ring. Tyr264 is well-known for UV-cross-linking to 8-azido ATP (*40*), which could occur if the adenine ring, with the 8-azido group attached to the C8 atom, moved to the syn conformation. In other structures of RecA, including the MnAMP−PNP complex described below, Tyr264 is rotated differently to contact the O2′ hydroxyl of the ribose moiety. The density for this side chain is slightly weaker than for most of the structure, consistent with its being somewhat flexible. There are no direct hydrogen bonds to the ribose hydroxyl groups of ADP, although the side chains of Ser240 and Arg227 are within about 4−5 Å and could conceivably form interactions with them with only slight conformational changes. The ring oxygen (O4′) of the ribose of ADP is within hydrogen-

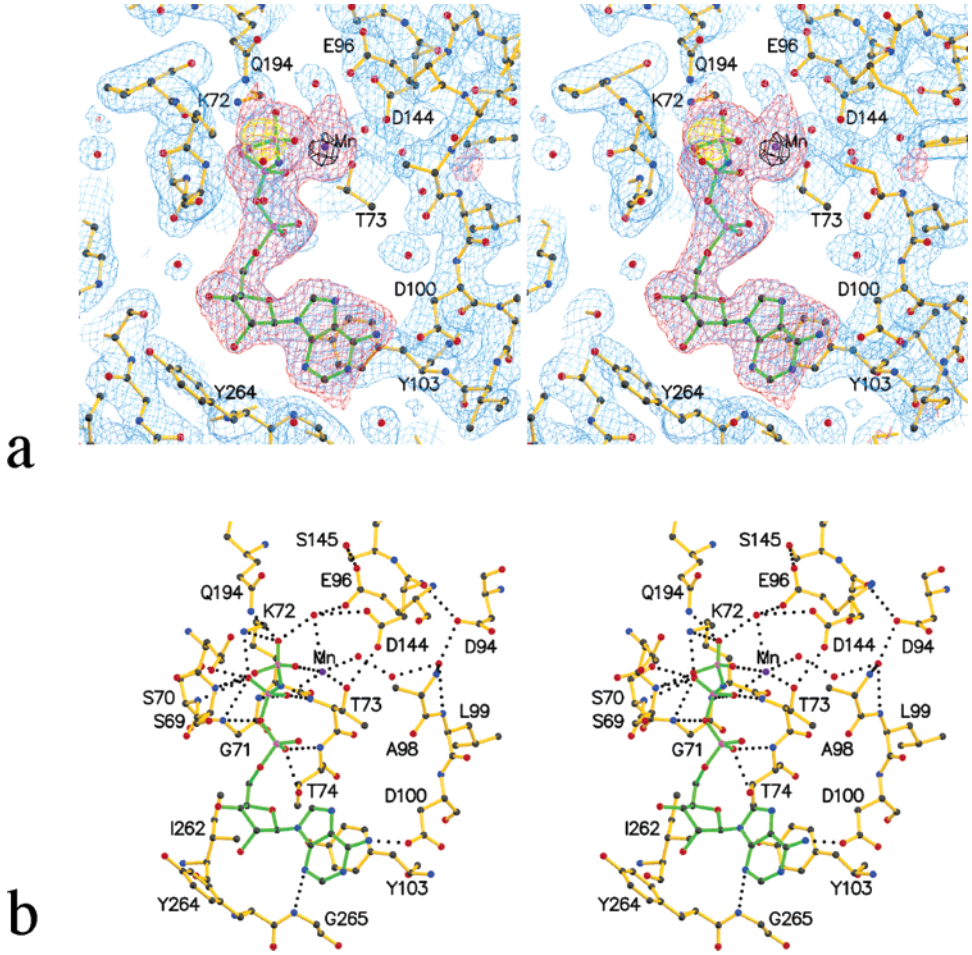

FIGURE 4: Interactions between RecA and MnAMP−PNP. (a) Stereoview of electron density in the vicinity of the bound MnAMP−PNP. The blue cage is a 2.1 Å $2F_{obs} - F_{calc}$ electron density map, contoured at 1 σ. The red cage is a simulated annealing $F_{obs} - F_{calc}$ omit map contoured at 3 σ, in which the manganese and AMP−PNP were omitted. The black cage is a RecA−MnAMP−PNP − RecA−MgAMP−PNP difference Fourier map contoured at 10 σ, showing a peak overlapping the position of the magnesium ion. The yellow cage is a RecA−MnAMP−PNP − RecA−MnADP difference Fourier map contoured at 10 σ, showing a peak overlapping the position of the γ phosphate of AMP−PNP. The view is roughly the same as in Figure 1b. Notice that the γ phosphate of AMP−PNP points out to the solvent (toward the viewer). (b) Stereoview of atomic interactions between RecA and MnAMP−PNP. Potential hydrogen bonds within 3.5 Å are shown as dotted lines.

bonding distance of the Oγ1 atom of Thr74 and is also near Tyr103.

Finally, a fifth region of RecA that approaches the active site is Gln194, located at the end of β-strand 5 and immediately preceding the disordered DNA-binding loop L2. Gln194 is thought to be a key mediator of the allosteric effect of ATP (*41*−*42*). Here, Gln194 does not contact the ADP directly but comes within about 4 Å of the β phosphate of ADP. Weak electron density for the side chain of Gln194 indicates that it is flexible. Overall, the ADP buries 65% (370 Å^2) of its surface area upon binding to RecA, leaving one side partially exposed to the solvent. Moreover, the binding pocket is not perfectly complementary to ADP, leaving some open space, particularly in the region between the α phosphate and the adenine ring (Figure 3a). Presumably, when the ATP moves to the subunit interface in the extended conformation, it becomes more fully buried, making additional close contacts with the enzyme, as is seen for RadA (*16*).

Structure of the RecA−MnAMP−PNP Complex. The electron density for the AMP−PNP is very complete, allowing for unambiguous positioning of the entire cofactor (Figure 4). A strong peak in the electron density allowed for accurate positioning of the manganese atom, which was confirmed by a 13 σ peak in a MnAMP−PNP − MgAMP−PNP ($F_{obs} - F_{obs}$) difference Fourier electron density map. Similarly, the position of the γ phosphate of AMP−PNP was confirmed by a 14 σ peak in a MgAMP−PNP − MgADP ($F_{obs} - F_{obs}$) difference Fourier map. The presence of the γ phosphate in AMP−PNP does not cause any significant conformational changes to occur, relative to the ADP-bound structure, and the ADP portion of AMP−PNP makes essentially all of the same contacts with the protein as does ADP. One small difference is seen for the side chain of Tyr264, which is rotated to contact the ribose hydroxyls of AMP−PNP, whereas it is rotated to contact the adenine ring in the ADP complex. Apparently this side chain, which is nearly invariant, is conformationally flexible, at least in the compressed, inactive state of the RecA filament. The γ phosphate of AMP−PNP, which points out to the solvent, forms contacts with the manganese ion, the backbone amide of Ser69, the side chains of Lys72 and Gln194, and 2 water molecules. Also nearby are the carboxylate groups of Glu68 and Glu96. Gln194 is thought to be a key sensor of the γ phosphate of ATP, relaying allosteric information from the ATP site to the loop L2 residues (195−209), which are a

primary ssDNA-binding site. The position of Gln194 is the same in the MnAMP−PNP and MgADP complexes. The electron density for Gln194 is somewhat weak, and the loop L2 residues remain disordered. Thus, although Gln194 does appear to contact the γ phosphate directly, it seems likely that the key role it plays in relaying the ATP-mediated conformational change is not fully revealed in this structure.

Lys72 and Glu96 are two residues that are thought to participate directly in ATP hydrolysis (*43*−*44*). By analogy with other ATPase enzymes, Glu96 is likely to be a catalytic base that activates a water molecule for nucleophilic attack on the γ phosphate, while Lys72 stabilizes the transition state of the hydrolysis reaction. While Lys72 contacts the γ phosphate of AMP−PNP directly, Glu96 is about 4 Å away. The side chain of Ser145 of the Walker B motif forms a close hydrogen bond (2.9 Å) with the carboxylate of Glu96, perhaps helping to precisely position it for catalysis. The carboxylate groups of Asp144 and Glu96 are within 4.2 Å of one another, likely raising the pK_a of Glu96, allowing it to function as a catalytic base. A water molecule that sits on top of the manganese atom and also contacts the γ phosphate and the side chains of Glu96 and Asp144 seems poised to attack the γ phosphate of AMP−PNP. The conformation of the AMP−PNP that best fits the electron density positions the γ phosphate with the open end pointing away from this water molecule, such that it is not poised for an in-line attack. Conceivably, the presence of the N3β atom of AMP−PNP, which is close to the manganese ion, could distort the positioning of the γ phosphate relative to the way ATP would bind. Alternatively, the appropriate geometry for ATP hydrolysis may fall into place only in the extended, active conformation of the protein, in which ATP is at the subunit interface. Because the ATPase activity of RecA is DNA-dependent, the correct geometry for ATP hydrolysis may also require bound DNA, which could promote a different position of the side chain of Gln194 than is observed here. In the structure of archaeal RadA bound to MgAMP−PNP in an extended conformation with AMP−PNP at the subunit interface, the conformation of AMP−PNP is such that the γ phosphate is better positioned for an in-line attack by a similarly positioned water molecule (*16*). In this structure, which does not have bound DNA, the DNA-binding loop L2 is disordered and Gln257, which corresponds to Gln194 of RecA, is positioned within 4 Å of the γ phosphate of AMP−PNP and the putative-hydrolyzing water molecule, as seen here for RecA−AMP−PNP.

It is interesting to compare the structure of the RecA−MnAMP−PNP complex reported here with a model of the RecA−MgATP complex proposed by Story and Steitz that was based on the structure of the RecA−ADP complex and other ATPase and GTPase enzymes (*7*). The structure and model share many common features, such as the interaction of Lys72 with the γ and β phosphates, the coplanar interactions of Thr73 and the γ and β phosphates with magnesium ion, the proximity of the Gln194 side chain to the γ phosphate, and the interaction of the carboxylate of Glu96 with a water molecule near the γ phosphate. Features of the structure determined here that were not emphasized in the model include the proximity of Asp144 of the Walker B motif to the carboxylate of Glu96 and the putative catalytic water molecule and the interaction of the γ phosphate with the backbone amide of Ser69 of the P loop. In the structure, the γ phosphate is not positioned for in-line attack, although the precise geometry is likely different in an active complex with loop L2 of RecA ordered on the bound DNA and ATP at the subunit interface.

Model of the Active Form of the RecA−MnAMP−PNP Complex. Disulfide cross-linking experiments indicated that there are ATP-mediated changes in the subunit interface in the RecA filament, as well as differences between the interactions that exist in solution and the interface that is observed in the original RecA crystal structure (*45*−*46*). Fitting of a RecA monomer from the crystal structure into density derived from 18 Å EM image reconstructions of extended RecA−DNA filaments provided a pseudoatomic model for the active form of the RecA filament, in which the ATP site is located in the subunit interface (*14*). The model explained the large cooperativity in ATP hydrolysis, and it was noted that several highly conserved residues, including Phe217, Lys216, Lys250, Arg222, Lys248, and Pro254, are brought to the subunit interface to close over the ADP that is bound in the active site of the neighboring subunit. The model also nicely accounted for the enhanced cooperativity of a Phe217Tyr version of RecA (*47*), which was puzzling based on its position in the original RecA structure. Recent crystal structures of extended archaeal RadA (*16*) and yeast Rad51 (*15*) filaments have the ATP site at the subunit interface, as seen in the EM model for RecA. In presenting the RadA structure, which includes bound MgAMP−PNP, it was noted that a highly conserved proline residue (Pro254 of *E. coli* RecA) closes over the active site to contact the adenine ring. The Rad51 structure is unique in that two distinct subunit interfaces are observed, indicating that there is a built-in asymmetry in the intersubunit interactions that may be mechanistically relevant.

Although the structure of the RecA−AMP−PNP complex presented here is clearly in the compressed, inactive conformation, it is possible to construct a model of the active form of the RecA−AMP−PNP complex (Figure 5) that is based on the recently reported structure of the extended form of the RadA−MgAMP−PNP complex in which the AMP−PNP is at the subunit interface (*16*). This model is similar to the one constructed for the active form of *E. coli* RecA by Wu et al. (*16*), except now the model is based on the 2.1 Å structure of RecA reported here that includes bound MnAMP−PNP. Although there are some steric clashes in this model, most of them, aside from those involving the N-terminal domain, could be alleviated by reorientations of the side chains and small movements of the backbone. There are several interesting features that come to light from this model that have not been discussed previously. For instance, the side chains of Lys248 and Lys250 from the neighboring subunit project into the active site to potentially interact with the phosphates of AMP−PNP. In fact, in the model, the Nζ atom of Lys248 approaches to within 3.0 Å of the γ phosphate of AMP−PNP and thus would appear to be suitably positioned to function in stabilizing the transition state of ATP hydrolysis, much like the "Arginine finger" that extends across the subunit interface of other ATPase and GTPase enzymes (*48*). Lys248 is invariant among bacterial RecA enzymes and when substituted to alanine results in the RecA protein with no ATPase or DNA strand-exchange activity (*49*). Lys250 is also invariant, and in the model, this residue approaches to within 3.2 Å of the α and

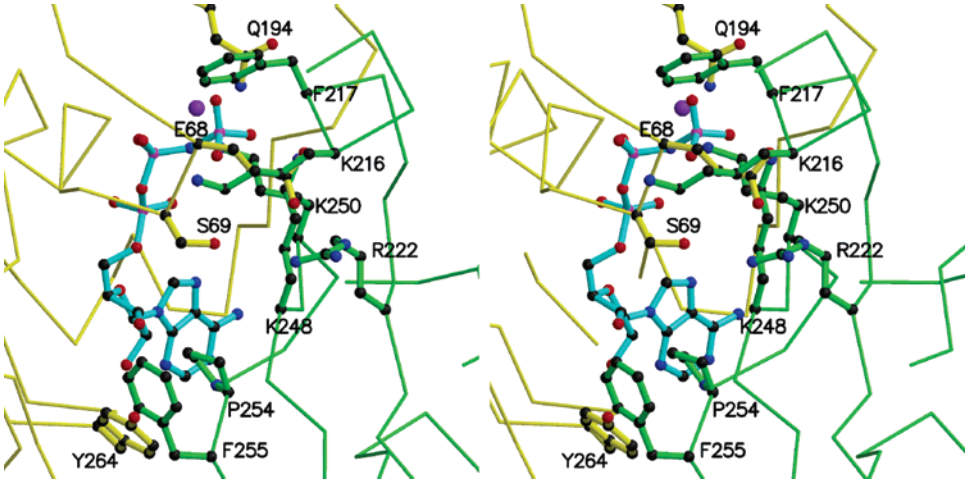

FIGURE 5: Close-up view of a model of the active form of *E. coli* RecA with bound AMP−PNP at the subunit interface. Starting with the coordinates of the RadA−AMP−PNP subunit in the asymmetric unit (PDB code 1T4G; *16*), a neighboring subunit was generated by the crystal symmetry to form a dimer. Then, the structure of the RecA−MnAMP−PNP complex determined here was superimposed onto both subunits of the RadA dimer, to generate a RecA dimer with the AMP−PNP at the subunit interface. The subunit with bound MnAMP−PNP is shown as a yellow Cα trace, and the neighboring subunit from the model is shown in green. Highly conserved amino acid residues that make contacts at the interface are shown in a ball-and-stick model. Steric clashes are evident in the model because it has not been energy-minimized. Notice that the ϵ-amino groups of Lys248 and Lys250 of the neighboring subunit approach the γ phosphate of AMP−PNP.

γ phosphates. Interestingly, similarly positioned positively charged residues are not also seen in the RadA structure. In fact, in the RadA structure, there are no direct interactions between the γ phosphate of AMP−PNP and side chains of the neighboring subunit. Instead, a network of water-mediated interactions is formed between the α and γ phosphates of AMP−PNP and Asp302 and Arg285 of RadA, which correspond to Lys248 and Arg222 of RecA, respectively. Thus, it is not obvious from the RadA structure how AMP−PNP (as opposed to ADP) causes the subunit reorientation that moves the ATP site to the subunit interface. Along these lines, it would be interesting to view a structure of RadA in a compressed, inactive form with bound ADP.

At the periphery of the ATP-binding site in the model of the active form of the *E. coli* RecA−MnAMP−PNP complex, several invariant or nearly invariant residues are brought near one another at the interface. While Phe217, Lys216, Lys250, Arg222, Lys248, and Pro254 have already been mentioned based on the EM model (*14*), it is apparent from the model in Figure 5 that Glu68, Ser69, Tyr264, and Phe255 should also be added to this list. All of these residues are invariant or nearly invariant, yet their functional roles are not obvious from their positions in the original *E. coli* RecA structure. The model of the active state of RecA−AMP−PNP would suggest that these residues are likely to be involved in interactions that stabilize the subunit interface in the active form of the filament. In the case of Glu68 and Ser69, their sensitivity to certain amino acid substitutions is consistent with such a role (*37*). Another residue of interest that is positioned near the interface in this model is Gln257. Gln257 is the site of a suppressor of RecF mutation (Gln257Pro; *50*) that may enhance binding of RecA to DNA. Conceivably, the Gln257Pro substitution could lead to stabilization of the interface, either by altering the conformation of the β7−β8 hairpin on which it lies or through contacts with the nearby β6−β7 hairpin of the neighboring subunit, to which it is brought near in the model.

It should be noted that similar models of the active form of the RecA−MnAMP−PNP complex can be constructed based either on the 18 Å EM reconstructions of extended RecA−DNA complexes (PDB code 1N03; *14*) or on the X-ray structure of yeast Rad51 with a pitch of 130 Å (PDB code 1SZP; *15*). In the case of Rad51, two such models can be constructed, because there are two distinct alternating interfaces observed in the filament in the crystal structure. Each of these models has AMP−PNP located at the subunit interface, but the detailed intersubunit interactions seen in the four models are quite different. For example, while Lys248 and Lys250 are close to the γ phosphate of AMP−PNP in the model based on the extended RadA structure, they are each >8 Å from the γ phosphate in the model based on the EM data (*14*), which instead has Lys216, Phe217, and Asn213 near the γ phosphate of AMP−PNP. In the model for the active state of RecA that is based on the structure of an extended yeast Rad51 filament, the side chains of Lys248 and Lys250 are 5−6 Å from the γ phosphate. Because predicting detailed interactions from these models is speculative, a high-resolution structure of *E. coli* RecA in the active form is needed to discern the detailed interactions and potential roles of the conserved residues.

CONCLUSIONS

The structures of *E. coli* RecA bound to MnAMP−PNP and MgADP, determined at 2.1 and 1.9 Å, respectively, provide a significantly more detailed view of the interactions between RecA and adenine nucleotides than has been available from other RecA structures. In particular, the interactions involving the magnesium ion are now clear as are the positions of several associated water molecules, one of which appears suitably positioned to participate directly in the ATP-hydrolysis reaction. This allows for a more precise assessment of the possible roles that each of the individual residues in the vicinity of the active site might have in promoting ATP hydrolysis and DNA strand exchange. On the basis of the crystallization and coprotease

experiments presented herein, as well as on structural information from EM of RecA−DNA filaments and recent crystal structures of Rad51 and RadA in the extended form, it seems clear that the structure of the AMP−PNP complex determined here does not represent the active conformation of the protein. Rather, it would appear that this structure represents a "preisomerization" state of the RecA−ATP complex, before the conformational change that moves the ATP site to the subunit interface has taken place. While a high-resolution view of the extended, active conformation of *E. coli* RecA remains elusive and would be most informative, a characterization of the conformational changes in RecA that takes place at all stages of the ATP binding and hydrolysis cycle will be necessary for a complete understanding of how RecA promotes the DNA strand-exchange reaction. Toward this end, the structures reported here provide a detailed view of what appears to be the ADP state, as well as the state after ATP binding but prior to isomerization to the active form.

ACKNOWLEDGMENT

Use of the Argonne National Laboratory Structural Biology Center beamlines at the Advanced Photon Source was supported by the U.S. Department of Energy, Office of Energy Research, under contract no. W-31-109-ENG-38. We thank Dr. Yu Luo for making coordinates of the crystal structure of the RadA−MgAMP−PNP complex available prior to publication.

REFERENCES

1. Roca, A. I., and Cox, M. M. (1997) RecA protein: Structure, function, and role in recombinational DNA repair, *Prog. Nucleic Acid Res. Mol. Biol. 56*, 129−223.
2. Kowalczykowski, S. C., Dixon, D. A., Eggleston, A. K., Lauder, S. D., and Rehrauer, W. M. (1994) Biochemistry of homologous recombination in *Escherichia coli*, *Microbiol. Rev. 58*, 401−465.
3. Roberts, J. W., Roberts, C. W., and Craig, N. L. (1978) *Escherichia coli rec*A gene product inactivates phage λ repressor, *Proc. Natl. Acad. Sci. U.S.A. 75*, 4714−4718.
4. Little, J. W. (1984) Autodigestion of LexA and phage λ repressors, *Proc. Natl. Acad. Sci. U.S.A. 81*, 1375−1379.
5. Egelman, E. H., and Stasiak, A. (1993) Electron microscopy of RecA−DNA complexes: Two different states, their functional significance and relation to the solved crystal structure, *Micron 24*, 309−324.
6. Story, R. M., Weber, I. T., and Steitz, T. A. (1992) The structure of the *E. coli rec*A protein monomer and polymer, *Nature 355*, 318−325.
7. Story, R. M., and Steitz, T. A. (1992) Structure of the recA protein−ADP complex, *Nature 355*, 374−376.
8. Menetski, J. P., and Kowalczykowski, S. C. (1985) Interaction of recA protein with single-stranded DNA. Quantitative aspects of binding affinity modulation by nucleotide cofactors, *J. Mol. Biol. 181*, 281−295.
9. Datta, S., Prabu, M. M., Vaze, M. B., Ganesh, N., Chandra, N. R., Muniyappa, K., and Vijayan, M. (2000) Crystal structures of *Mycobacterium tuberculosis* RecA and its complex with ADP−AlF_4: Implications for decreased ATPase activity and molecular aggregation, *Nucleic Acids Res. 28*, 4964−4973.
10. Datta, S., Ganesh, N., Chandra, N. R., Muniappa, K., and Vijayan, M. (2003) Structural studies on MTRecA−nucleotide complexes: Insights into DNA and nucleotide binding and the structural signature of NTP recognition, *Proteins: Struct., Funct., Genet. 50*, 474−485.
11. Datta, S., Krishna, R., Ganesh, N., Chandra, N. R., Muniyappa, K., and Vijayan, M. (2003) Crystal structures of *Mycobacterium smegmatis* RecA and its nucleotide complexes, *J. Bacteriol. 185*, 4280−4284.
12. Xing, X., and Bell, C. E. (2004) Crystal structures of *Escherichia coli* RecA in a compressed helical filament, *J. Mol. Biol. 342*, 1471−1485.
13. Rajan, R., and Bell, C. E. (2004) Crystal structure of RecA from *Deinococcus radiodurans*: Insights into the structural basis of extreme radioresistance, *J. Mol. Biol. 344*, 951−963.
14. VanLoock, M. S., Yu, X., Yang, S., Lai, A. L., Low, C., Campbell, M. J., and Egelman, E. H. (2003) ATP-mediated conformational changes in the RecA filament, *Structure 11*, 187−196.
15. Conway, A. B., Lynch, T. W., Zhang, Y., Fortin, G. S., Fung, C. W., Symmington, L. S., and Rice, P. A. (2004) Crystal structure of a Rad51 filament, *Nat. Struct. Biol. 11*, 791−796.
16. Wu, Y., He, Y., Moya, I. A., Qian, X., and Luo, Y. (2004) Crystal structure of archaeal recombinase RadA: A snapshot of its extended conformation, *Mol. Cell 15*, 423−435.
17. Cox, M. M. (2003) The bacterial RecA protein as a motor protein, *Annu. Rev. Microbiol. 57*, 551−577.
18. Aihara, H., Ito, Y., Kurumizaka, H., Terada, T., Yokoyama, S., and Shibata, T. (1997) An interaction between a specified surface of the C-terminal domain of RecA protein and double-stranded DNA for homologous pairing, *J. Mol. Biol. 274*, 213−221.
19. Malkov, V. A., and Camerini-Otero, R. D. (1995) Photo cross-links between single-stranded DNA and *Escherichia coli* RecA protein map to loops L1 (amino acid residues 157−164) and L2 (amino acid residues 195−209), *J. Biol. Chem. 270*, 30230−30233.
20. Egelman, E. H., and Yu, X. (1989) The location of DNA in RecA−DNA helical filaments, *Science 245*, 404−407.
21. Soultanas, P., and Wigley, D. B. (2000) DNA helicases: "Inching forward", *Curr. Opin. Sruct. Biol. 10*, 124−128.
22. Abrahams, J. P., Leslie, A. G. W., Lutter, R., and Walker, J. E. (1994) Structure at 2.8 Å resolution of F1-ATPase from bovine heart mitochondrial, *Nature 370*, 621−628.
23. Chang, G., and Roth, C. B. (2001) Structure of MsbA from *E. coli*: A homolog of the multidrug resistance ATP binding cassette (ABC) transporters, *Science 293*, 1782−1784.
24. Locher, K. P., Lee, A. T., and Rees, D. C. (2002) The *E. coli* BtuCD structure: A framework for ABC transporter architecture and mechanism, *Science 296*, 1038−1040.
25. Hopfner, K. P., Karcher, A., Shin, D. S., Craig, L., Arthur, L. M., Carney, J. P., and Tainer, J. A. (2000) Structural biology of Rad50 ATPase: ATP-driven conformational control in DNA double-strand break repair and the ABC-ATPase superfamily, *Cell 101*, 789−800.
26. Bell, C. E., Frescura, P., Hochschild, A., and Lewis, M. (2000) Crystal structure of the λ repressor C-terminal domain provides a model for cooperative operator binding, *Cell 101*, 801−811.
27. Otwinowski, Z., and Minor, W. (1997) Processing of X-ray diffraction data collected in oscillation mode, *Methods Enzymol. 276*, 307−326.
28. Navaza, J. (1994) AMoRe: An automated package for molecular replacement, *Acta Crystallogr., Sect. A 50*, 157−163.
29. Collaborative Computational Project Number 4 (1994) The *CCP*4 suite: Programs for protein crystallography, *Acta Crystallogr., Sect. D 550*, 760−763.
30. Brünger, A. T., Adams, P. D., Clore, G. M., DeLano, W. L., Gros, P., Grosse-Kunstleve, R. W., Jiang, J. S., Kuszewski, J., Nilges, M., Pannu, N. S., Read, R. J., Rice, L. M., Simonson, T., and Warren, G. L. (1998) Crystallography and NMR system: A new software suite for macromolecular structure determination, *Acta Crystallogr., Sect. D 54*, 905−921.
31. Jones, T. A., Zhou, J.-Y., Cowan, S. W., and Kjeldgaard, M. (1991) Improved methods for building protein models in electron density maps and the location of errors in these models, *Acta Crystallogr., Sect. A 47*, 110−119.
32. Kraulis, P. (1991) MOLSCRIPT: A program to produce both detailed and schematic plots of protein structures, *J. Appl. Crystallogr. 24*, 946−950.
33. Merritt, E. A., and Bacon, D. J. (1997) Raster3D: Photorealistic molecular graphics, *Methods Enzymol. 277*, 505−524.
34. McKay, D. B., Steitz, T. A., Weber, I. T., West, S. C., and Howard-Flanders, P. (1980) Crystallization of monomeric RecA protein, *J. Biol. Chem. 255*, 6662.
35. Karlin, S., and Brocchiere, L. (1996) Evolutionary conservation of RecA genes in relation to protein structure and function, *J. Bacteriol. 178*, 1881−1894.

36. McGrew, D. A., and Knight, K. L. (2003) Molecular design and functional organization of the RecA protein, *Crit. Rev. Biochem. Mol. Biol. 38*, 385−432.
37. Konola, J. T., Logan, K. M., and Knight, K. L. (1994) Functional characterization of residues in the P-loop motif of the RecA ATP binding site, *J. Mol. Biol. 237*, 20−34.
38. Stole, E., and Bryant, F. R. (1996) Reengineering the nucleotide cofactor specificity of the RecA protein by mutation of aspartic acid 100, *J. Biol. Chem. 271*, 18326−18328.
39. Yu, X., Jacobs, S. A., West, S. C., Ogawa, T., and Egelman, E. H. (2001) Domain structure and dynamics in the helical filaments formed by RecA and Rad51 on DNA, *Proc. Natl. Acad. Sci. U.S.A. 98*, 8419−8424.
40. Knight, K. L., and McEntee, K. (1985) Tyrosine 264 in the recA protein from *Escherichia coli* is the site of modification by the photoaffinity label 8-azidoadenosine 5′-triphosphate, *J. Biol. Chem. 260*, 10185−10191.
41. Kelley, J. A., and Knight, K. L. (1997) Allosteric regulation of RecA protein function is mediated by Gln^{194}, *J. Biol. Chem. 272*, 25778−25782.
42. Voloshin, O. N., Wang, L., and Camerini-Otero, R. D. (2000) The homologous pairing domain of RecA also mediates the allosteric regulation of DNA binding and ATP hydrolysis: A remarkable concentration of functional residues, *J. Mol. Biol. 303*, 709−720.
43. Rehrauer, W. M., and Kowalczykowski, S. C. (1993) Alteration of the nucleoside triphosphate (NTP) catalytic domain within *Escherichia coli* recA protein attenuates NTP hydrolysis but not joint molecule formation, *J. Biol. Chem. 268*, 1292−1297.
44. Campbell, M. J., and Davis, R. W. (1999) On the *in vivo* function of the RecA ATPase, *J. Mol. Biol. 286*, 437−445.
45. Skiba, M. C., Logan, K. M., and Knight, K. L. (1999) Intersubunit proximity of residues in the RecA protein as shown by engineered disulfide cross-links, *Biochemistry 38*, 1193−11941.
46. Logan, K. M., Forget, A. L., Verderese, J. P., and Knight, K. L. (2001) ATP-mediated changes in cross-subunit interactions in the RecA protein, *Biochemistry 40*, 11382−11389.
47. De Zutter, J. K., Forget, A. L., Logan, K. M., and Knight, K. L. (2001) Phe217 regulates the transfer of allosteric information across the subunit interface of the RecA protein filament, *Structure 9*, 47−55.
48. Wittinghofer, A. (1998) Signal transduction via ras, *Biol. Chem. 379*, 933−937.
49. Nguyen, T. T., Muench, K. A., and Bryant, F. R. (1993) Inactivation of the recA protein by mutation of histidine 97 or lysine 248 at the subunit interface, *J. Biol. Chem. 268*, 3107−3113.
50. Wang, T. C., Madiraju, M. V., Templin, A., and Clark, A. J. (1991) Cloning and preliminary characterization of srf-2020 and srf-801, the recF partial suppressor mutations which map in recA of *Escherichia coli* K-12, *Biochimie 73*, 335−340.

BI048165Y